Journal of
Mechanical
Science and
Technology

Journal of Mechanical Science and Technology 21 (2007) 549~555

Numerical and Experimental Study on a Channel Mixer with a Periodic Array of Cross Baffles

Yong Kweon Suh[a,*], Seong Gyu Heo[a], Young Gun Heo[a],
Hyeung Seok Heo[a], Sangmo Kang[a]

[a]*Department of Mechanical Engineering, Dong-A University, 840 Hadan-dong, Saha-gu, Busan 604-714, Korea*

(Manuscript Received May 24, 2006; Revised January 25, 2007; Accepted January 27, 2007)

Abstract

In this study we show an enhanced mixing effect with a simple channel having a periodic array of cross baffles. We performed numerical computation to obtain the steady flow field within the channel at low Reynolds numbers by using a commercial code, ANSYS CFX 10.0. A visualization experiment was also conducted to validate our numerical results qualitatively. In evaluating the mixing performance, we employed the Lyapunov exponent. It was shown that the visualized mixing pattern was in a good agreement with that numerically given. Our Liapunov exponent distribution in the space also demonstrates that the proposed channel design indeed exhibits a chaotic stirring at low Reynolds numbers. Our design is thus assumed to be applicable to designing a microchannel mixer with enhanced mixing effect.

Keywords: Channel mixer, Baffle, Poincare section, Lyapunov exponent, Chaotic advection, Saddle point

1. Introduction

Recently there have been significant advances in development of MEMS (Microelectromechanical System) and bio-technology associated with LOC (lab-on-a chip). The advantages of micro-systems when they are applied to LOC are well known. They consume very little amount of reagents in the processing such as sorting, separation, reaction, and detection, etc. These sub-processes can be integrated into one small but global micro-system, so that it is even very easy to handle.

In this case, the uttermost important thing is how to mix the reagents fast and effectively; in micro scales the fluid turbulence in most cases cannot be expected to occur because the relevant Reynolds numbers are very small. Increasing the contact surface between different fluids by controlling fluid flows within the channel is very important to enhance the mixing. In laminar flows, this can be achieved by the mechanism represented by the well known concept "chaotic advection" (Suh, 1995). Aref (2002) studied the mixing effect provided by the microchannel of a serpentine type. Bertsch et al. (2001) fabricated a mixer made by crossing two helical-type channels and studied the mixing effect in terms of the chaotic stirring. Stroock et al. (2002) exhibited the chaotic advection within the microchannel of staggered herringbone type mixer. The fundamental studies on using the various tools of chaotic advection were performed by Suh & Moon (1994) and Moon and Suh (1994). Heo and Suh (2005) presented a newly invented microchannel having relatively high blocks periodically attached on the bottom wall of the channel and they demonstrated an efficient mixing. On the other hand, Suh et al. (1997) and Suh (2004) investigated numerically the mixing characteristics

*Corresponding author. Tel.: +82 51 200 7648, Fax.: +82 51 200 7656
E-mail address: yksuh@dau.ac.kr

within staggered channels in a model simulating a screw extruder.

In this paper we report the results of numerical as well as experimental studies on the mixing effect with a relatively simple design of channel mixer having crossed baffles attached periodically at the top and bottom walls. This channel is designed for the purpose to be used as a micromixer. Compared with the previously investigated micromixers this design is extremely simple and it provides the chaotic advection leading to significant mixing effect.

2. Flow Model and Numerical Methods

2.1 Flow model

Figure 1 shows the sketch of our flow model used in the present study. The length, width and height of channel are along the x, y, and z coordinates, respectively. In this study all the variables are dimensional. H and W denote the height and width of the channel cross-section, respectively, and P is the spatial period of the baffle array. Definitions of these and other geometric parameters as well as their dimensions are displayed in Table 1. The inlet length of the channel where no baffles are built is set as 150 [μm].

In this study, the Reynolds number is defined as

$$\mathrm{Re} = \frac{\rho V D_h}{\mu} \tag{1}$$

Here, V is the average velocity, ρ the density, μ the viscosity, and D_h the hydraulic diameter of the channel section. We fix the channel width as 100 [μm]. The fluid flow is assumed to obey the continuum hypothesis. Since the flow is very slow, it belongs to a Stokes flow regime.

Table 1. Geometric variables and their dimensions of the channel and the baffles.

Varianble	Dimension	Remarks
H	100 μm	height of the channel
W	100 μm	width of the channel
h	0.5H	height of the baffle
L	950 μm	total length of the channel
ℓ	1.5H	length of the baffle
t	0.05H	thickness of the baffle
g	0.1H	gap between the baffle and channel wall
P	2H	period of the baffle array

2.2 Numerical methods

Above all, we obtained the steady-state solutions of the Navier-Stokes equations by using the commercial code, ANSYS CFX 10.0. For this, we constructed a unstructured tetra-mesh-grid system for the 3-D flow domain with the number of grids up to 11,000,000.

As the inlet condition, a fully developed velocity profile is applied as given by Gondret et al. (1997);

$$u(y,z) = \frac{GW^2}{8\mu}\left\{1-(\frac{2y}{W})^2 + \sum_{n=1}^{\infty}(-1)^n \frac{32}{(2n-1)^3\pi^3} \times \frac{\cosh((2n-1)\pi(z/W)}{\cosh((2n-1)\pi/2H/2)}\cos((2n-1)\pi\frac{y}{W})\right\} \tag{2}$$

In Eq. (2), we need to provide the pressure gradient G, and this parameter is determined in such way that the section-average velocity becomes 500 [μm/s] for the case of a circular pipe with the pipe diameter 113[μm] that produces the same cross-sectional area as the rectangular section of the present channel model; the value of G is 1256[Pa/m]. Because the sectional shape of the pipe is rectangular, the average velocity is different from 500 [μm/s]; it was calculated to be 440 [μm/s]. The Reynolds number with this velocity is about 0.13.

As the outlet condition of the channel, we apply zero gradients along the downstream direction for all the physical variables. On the surface of the wall of

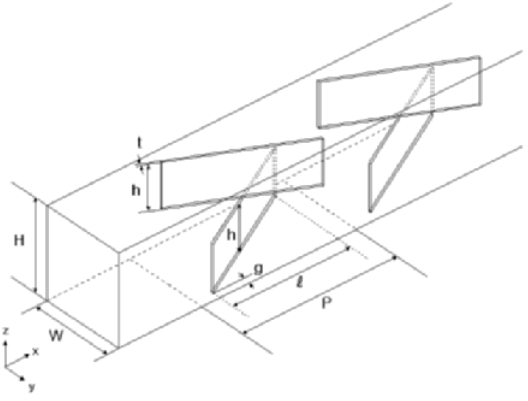

Fig. 1. Perspective view of the channel with blocks attached periodically to the bottom and top walls.

the channel and baffles, we apply the impermeable and no-slip boundary conditions.

Next, we get the streamlines (or pathlines) also by using the code's post-processor. Then, we obtained the Poincare sections and calculated the Lyapunov exponents to investigate the mixing performance.

The Poincare sections are in general useful in distinguishing between the good and poor mixing regions. However in this study we use these sections in establishing the numerical visualization of the mixing pattern for comparison with the experimental results. For this, we distributed passive particles at the half plane of the entrance section of the channel. Then the code gives the information of the streamlines starting at these initial positions. The Poincare section corresponds to the collection of points, given by the intersection of these streamlines and the target section of the channel. A linear interpolation was used in calculating the (y,z) coordinates of the inter-sections from the data of the coordinates for the streamlines.

In the chaotic region, distance between two fluid particles is increased exponentially in time. The degree of the stretching indicates the degree of mixing (Ottino, 1989). Lyapunov exponent is a temporally and spatially averaged value representing the exponential stretching of material blob in the flow field. Suppose we have a pair of particles initially $(t=0)$ at a distance l_o from each other. At a later time t, the distance becomes l. Then exponential stretching means that for a positive constant Λ the distance is determined by

$$l = l_o \exp(\Lambda t) \tag{3}$$

where Λ corresponds to the Lyapunov exponent. The distance of course may not show in practice such an exponential change at every instant of time. This means we must think that the distance follows the rule (3) in a time-average sense (usually long-time average). We can write Eq. (3) in the following form.

$$\Lambda = \lim_{t\to\infty} \frac{1}{t} \ln(l/l_o) \tag{4}$$

where long-time average was implied. The dimension of Lyapunov exponent is [1/s].

3. Experimental method in macro scales

Main purpose of this experiment is to validate the numerical results of the viscous flow and mixing characteristics. We performed the experiment in macro scales, because we assumed that there should be similarity between the micro- and macro-scale flows if the Reynolds number is very small for both cases. After all, flow visualization in the macro scale is much easier than in the micro scale.

Figure 2 shows the experimental apparatus for visualization of the flow in the channel. Upstream of the visualization channel, a T-shape guide-channel is attached. Each of the other two ends of the guide channel is attached to a tank, one (tank 1) containing pure glycerin, and the other (tank 2) containing glycerin mixed with small amount of a fluorescent dye. We can control the flow rate by a discharge valve at the outlet of the channel(not shown in this figure). The argon-ion-laser sheet sheds light in a cross-sectional plane of the channel at a desired location for the flow visualization.

4. Results and discussions

Figure 3 shows the numerical results of the velocity field of the secondary flow in each section of the channel. The secondary flow is of circular motion moving counter-clockwise. This motion comes from the characteristics of the baffle structure as shown in the Fig. 1. If the baffles were mounted inversely (i.e. if the upper and lower baffles were exchanged), the secondary flow would show a clockwise motion. This

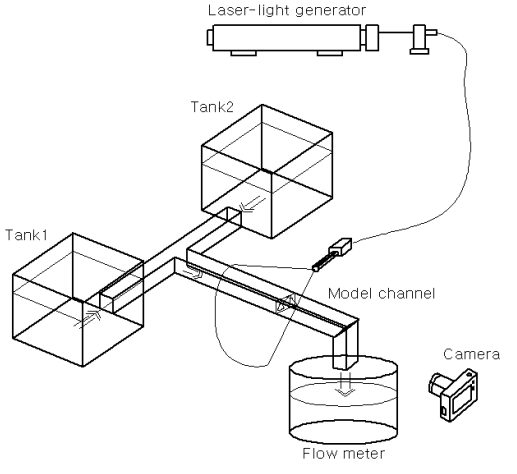

Fig. 2. Experimental apparatus for visualization of the viscous flow in the channel

secondary flow of course plays very important roles in fluid mixing. Intensity of the secondary flow is maximum at the sectional point where the upper and lower baffles meet each other, i.e. Fig. 3 (e). On the one hand, at the sectional plane where the baffles start to appear (Fig. 3(b)) and disappear (Fig. 3(h)), the secondary-flow field shows a hyperbolic shape and the saddle point is located at the center of each section. Coexistence of such circular and hyperbolic-type motions is indeed expected to lead to a good mixing (Ottino, 1989).

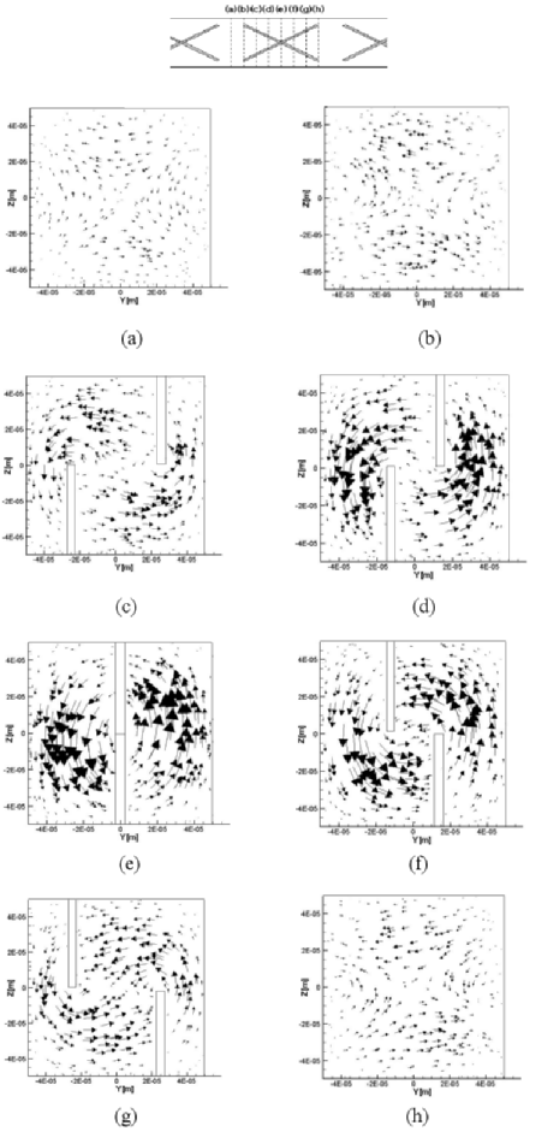

Fig. 3. Sectional view of the secondary-flow velocity vectors within the 3rd baffled space; viewed from the outlet side.

Figure 4 shows the streamlines given by the velocity field of the secondary flow in each section of the channel. As was seen from Fig. 3, the secondary flow is of circular motion moving counter-clockwise (Fig. 4b, c, d), and the position of saddle point is also clearly identified at the center (Fig. 4a, b, d).

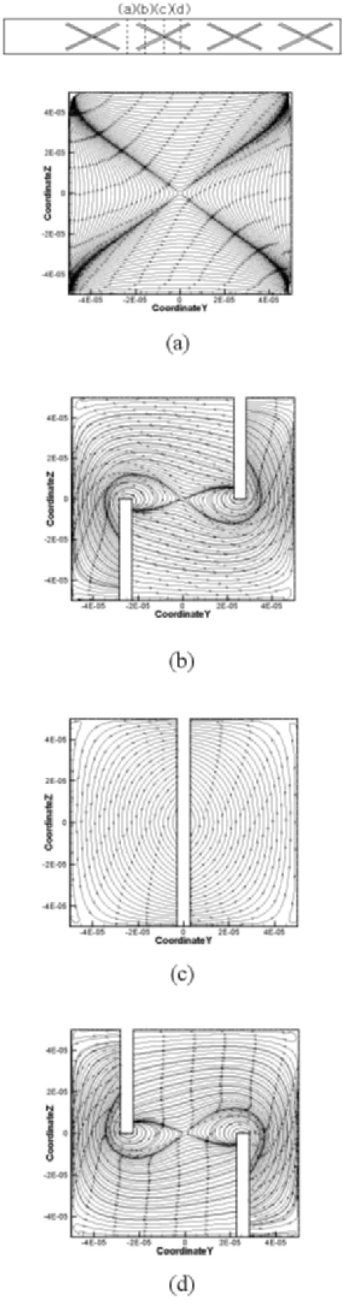

Fig. 4. Sectional view of the secondary-flow streamlines within the 2nd baffle space; viewed from the outlet side.

Figure 5 shows the Poincare sections given from the numerical computation (left-hand side pictures) in comparison with the results of flow visualization (right-hand side pictures). To obtain the Poincare sections, the particles are initially distributed at the entrance section of the channel only on the half region (i.e. the right-hand side viewed from downstream region). Collection of these particles at the desired sectional plane yields the Poincare section. The numerical results remarkably well reproduce the visualization results. This implies that our numerical methods as well as the results are reliable. We can see from these plots that the interface of the two different fluid phases elongates rapidly due to the characteristic secondary-flow motion described above. We may conjecture that there must be a stretching-folding mechanism (i.e. chaotic advection) responsible for the rapid stretching.

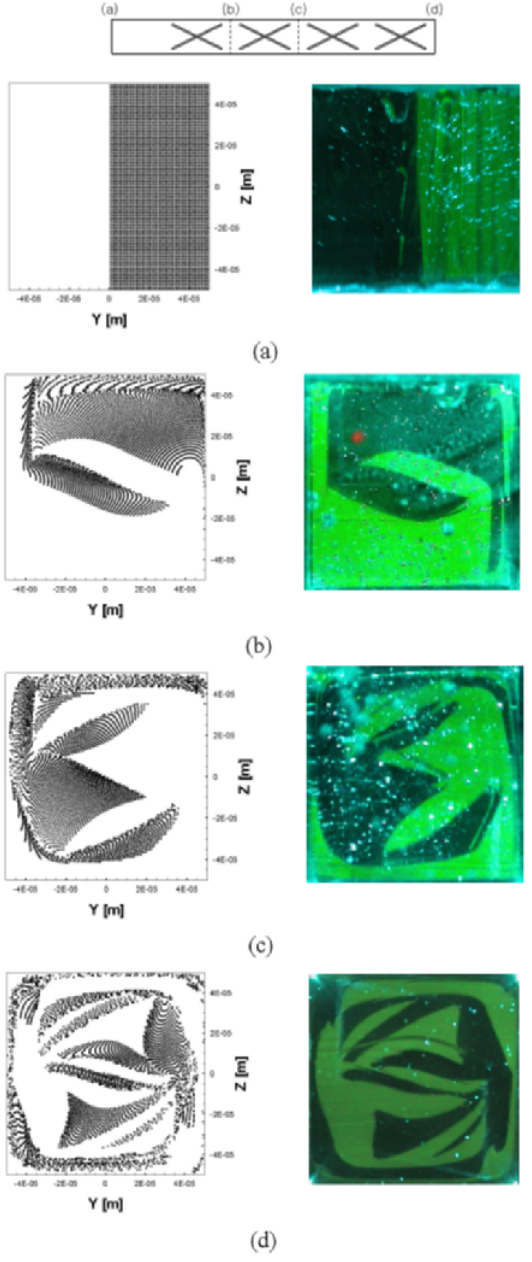

Fig. 5. Comparison of Poincare sections obtained numerically (left-hand side) and the cross-sectional views of the visualization experiment given from the experiment (right-hand side) in the channel.

Figure 6 shows distribution of the Lyapunov exponent obtained from the numerical computation. At first, 10000 pairs of passive particles are uniformly

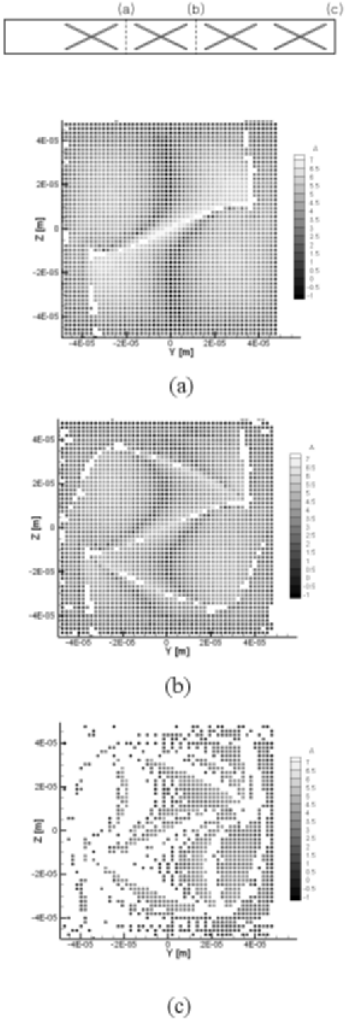

Fig. 6. Distribution of the Lyapunov exponent obtained numerically for the 4-period channel.

distributed at the inlet plane. The initial distance of each pair is 0.5μm separated in the y-direction. When each of the particle pairs arrives at the specific sectional plane, the Lyapunov exponent is computed by using the formula (4). Each dot shown in Fig. 6 denotes the Lyapunov exponent obtained at the corresponding initial point, the color indicating the magnitude. The points where no dots appear mean that the Lyapunov exponents cannot be obtained because one or both of the pair of particles didn't arrive at the target cross-section. This happens when the particle moves very slowly in close proximity to the wall of the channel or the baffles. Nevertheless, we can see that in overall the positive Lyapunov exponent is dominant. This means that the present baffle structure reveals a chaotic advection leading to an improved mixing performance.

Next, we computed the Lyapunov exponents from one spatially periodic flow field, i.e. the flow data taken from the 3rd baffled space. Usually the Lyapunov exponents are very high and decreasing rapidly at the initial time, and therefore to obtain the reliable data we must perform the calculation for large spatial or temporal periods. Figure 8 shows 81 initial positions used to measure the Lyapunov exponent for the spatially periodic channel described above. In each position, a pair of passive particles, located very close to each other, is ready to start the movement. When one of the pair particles arrives at the downstream end section, the distance between the particles is calculated and the temporal, local Lyapunov exponent is computed by using (4) with the time elapse t. Then the particles are brought again to the entrance plane keeping the coordinates y and z unchanged. In this way the computation was repeated for 20 times. In Fig. 8, the symbol "X" indicates that at least one of the corresponding particles did not arrive at the designated section without providing the Lyapunov exponent.

Figure 9 shows five typical histories of the Lyapunov exponents obtained at different initial positions. In overall the Lyapunov exponent is low when the particles are near to walls. Figure 10 shows the time history of the Liapunov exponent spatially averaged over 71 pair of particles (i.e. for the initial positions indicated by solid circles in Fig. 6). The data approaches a constant value 1.7 implying again that the proposed design provides a chaotic advection leading to a good mixing.

As shown above the numerical results indicate that the proposed channel design with cross baffles provides excellent mixing performance. However,

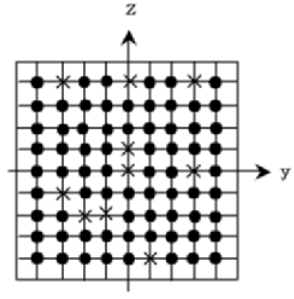

Fig. 8. Initial points of particles used in calculating the Lyapunov exponents for the spatially periodic channel constructed from the 3rd period channel data.

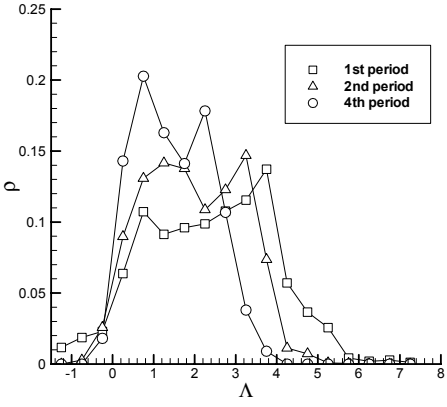

Fig. 7. Probability density of the Lyapunov exponent after 1st, 2nd, and 4th periods obtained numerically for the 4-period channel.

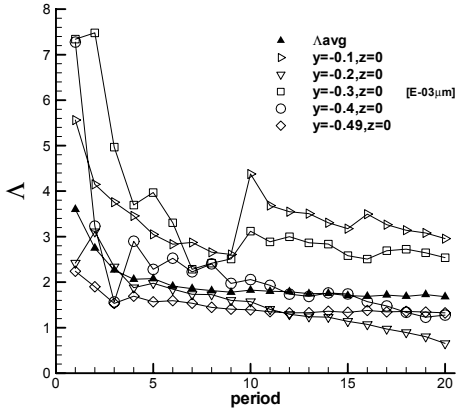

Fig. 9. Temporal change of the local Lyapunov exponents defined at several initial positions for the channel described in Fig. 8.

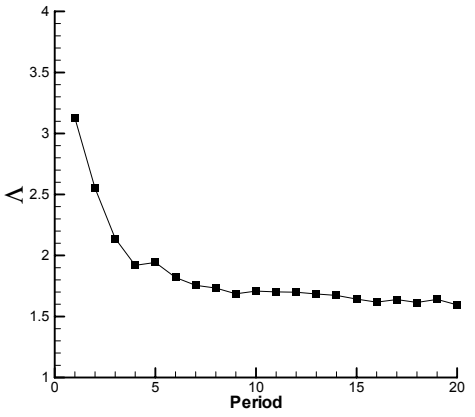

Fig. 10. Temporal change of the Lyapunov exponent averaged over the space for the same channel described in Fig. 8.

because of the baffles, the pressure gradient must increase for the same flow rate as the case without the baffles. The pressure drop over one spatial period, 200[μm], was found to be 0.829[Pa] with the baffles, while the case without the baffles gives 0.250[Pa]. Therefore increase of the pressure gradient due to the existence of the baffles is almost 2.3 times the original one.

5. Conclusions

We summarize our findings of the present study from the numerical and experimental results as follows.

(1) Poincare sections obtained by the numerical computation in the micro scales is in a remarkably good agreement with the flow visualization results obtained from the macro-scale experiments.

(2) The crossed-baffle structure proposed in this study reveals the circular as well as hyperbolic-type motion of particles which is responsible for the chaotic advection and exponential stretching of the material blobs.

(3) According to the results of the numerical computation, we can expect appearance of chaotic advection from the proposed channel mixer in view of the positive Lyapunov exponents dominant in the flow field.

Acknowledgements

This work was supported by the Korea Science and Engineering Foundation(KOSEF) through the National Research Laboratory Program funded by the Ministry of Science and Technology (No. 2005-1091).

References

Aref, H., 2002, "The Development of Chaotic Advection," *Phys. Fluids*, Vol. 14, pp. 1315~1325.

Bertsch, A., Heimingartner, S., Cousseau, P., 2001, "3D Micromixers-Downscaling Large Scale Industrial Static Mixers," Proc. *IEEE MEMS*, pp. 507~510.

Gondret, P., Rakotomalala, N., Rabaud, M., Salin, D., Watzky, P., 1997, "Viscous Parallel Flow in Finite Aspect Ratio Hele-Shaw Cell: Analytical and Numerical Results," *Phys. Fluids*, Vol. 9, No. 6, pp. 1841~1843.

Heo, H. S., Suh, Y. K., 2005, "Enhancement of Stirring in a Straight Channel at Low Reynolds-Number with Various Block-Arrangement," *J. Mech. Sci. Tech*., Vol. 19, No. 1, pp. 199~208.

Moon, J. C., Suh, Y. K., 1994, "Fluid Flow and Stirring in a Rectangular Tank-Effect of the Plate Length," *Trans. of the KSME(B)*, Vol. 18, No. 10, pp. 2698~2750.

Ottino, J. M., 1989, *The Kinematics of Mixing: Stretching, Chaos, and Transport*, Cambridge Univ. Press.

Stroock, A. D., Destinger, S. K. W., Ajdari, A., Mezic, I., Stone, H. A., Whitesides, G.. M., 2002, "Chaotic Mixer for Microchannels," *Science*, Vol. 295, pp. 647~651.

Suh, Y. K., 1995, "Chaotic Stirring of an Alternately-Driven-Cavity Flow," *Trans. of the KSME(B)*, Vol. 19, No. 2, pp. 537~547.

Suh, Y. K., 2004, "Analysis of the Stokes Flow and Stirring Characteristics in a Stagered Screw Channel," *J. Comput. Fluids Engng*, Vol. 9, No. 4, pp. 55~63.

Suh, Y. K., Moon, J. C., 1994, "Chaotic Stirring in a Shallow Rectangular Tank," *Trans. of the KSME(B)*, Vol. 18, No. 2, pp. 380~388.

Suh, Y. K. Kim, Y. K., Moon, J. C., 1997, "A Numerical Study on a Chaotic Stirring in a Model for a Single Screw Extruder," *Trans. of the KSME(B)*, Vol. 21, No. 12, pp. 1615~1623.